J. Fluid Mech. (2000), *vol.* 421, *pp.* 369–380. Printed in the United Kingdom

Flow-induced patterns in directional solidification: localized morphologies in three-dimensional flows

By Y.-J. CHEN AND S. H. DAVIS

Department of Engineering Sciences and Applied Mathematics
Northwestern University, Evanston, IL 60208, USA

(Received 19 January 2000)

We consider the effect of steady, three-dimensional cellular convective fields impressed upon the moving front of a dilute binary alloy in directional solidification. The flows have length scales longer than the characteristic lengths of the morphological instability. A Floquet problem with multiple degrees of freedom in space governs the interfacial dynamics and determines the morphological patterns and marginal stability boundaries. In the cases of weak flows the induced patterns are superpositions of rolls modulated by the forced flows. When the flows are strong, the instability becomes spatially localized and confined at inward flow-stagnation regions on the front. Numerical computations and the WKB method are used to solve the eigenvalue problems, showing various localized states depending on the structures of the imposed flows.

1. Introduction

A homogeneous state may bifurcate into spatial patterns when a control parameter of a physical system is raised above a critical value. A linear stability analysis that probes the evolution of infinitesimal disturbances to the uniform state delivers the stability threshold and spatial–temporal scales of the cellular structures. Often, this ideal scenario is compromised by a slowly varying parameter in the background, or perturbed by an external forcing that has a length scale long compared to that of the intrinsic cellular structure. In this situation multi-scale interaction can lead to spatially localized patterns, whose distribution is well-correlated with the long-scale variation. We present here a case in directional solidification of a binary alloy coupled with convection.

The study of forced flows over solidifying interfaces aims at examining the induced morphological patterns; the results have implications for the design of microstructures of materials by employing fluid motions. This goal has motivated many authors to investigate the flow-modified morphologies with prescribed flow fields. For example, Coriell, McFadden & Boisvert (1984) examined the effect of plane Couette flow; Forth & Wheeler (1989), Hobbs & Metzener (1991), and Schultze & Davis (1994) considered the case of asymptotic suction profile; Brattkus & Davis (1988) studied the instability induced by a stagnation-point flow (see also Davis 1993 for a review). For those cases the imposed flows redistribute solute in the melt, which modifies the stability boundary from the pure solidification problem. The morphological patterns are altered as well, depending on the imposed flow profiles.

In the present study we examine the morphological instabilities of solidification

fronts advancing into pre-existing cellular convective fields. The motions are three-dimensional, with prescribed spatial scales and magnitudes. The analogous two-dimensional flow problem has been studied previously (Chen & Davis 1999), with a conclusion that the flow promotes three-dimensional instability and produces localized patterns at the inward stagnation points of the cellular flow. Those stagnation regions are the positions where the interfacial flow converges and inhomogeneities accumulate. Here, we extend the previous results to three-dimensional flow systems. The flow fields near the free surface are then characterized by inward stagnation points or lines, which consequently result in a local focus- or ridge-like morphology, respectively. New types of morphological patterns are predicted and insights gained in our previous work allow us to deconstruct this more complex situation. The materials so produced possess a type of 'composite' structure induced by the cellular convective fields.

Problems of similar mathematical structures can be found in other physical systems, which include Bénard convection with a non-uniform heating (Pal & Kelly 1979; Walton 1982), band theory of solids (Connor *et al.* 1980), premixed flames in inhomogeneous flows (Class, Bühler & Davis 1998), and sedimentation in meandering channels (Eckhaus & Kuske 1997; Schielen & Doelman 1998). Most studies have considered parametric-excitation systems with a single degree of freedom (e.g. Mathieu's equation). By contrast, in the present study the resulting dynamics have Floquet structures with multiple degrees of freedom in space. Thus, in addition to the study of crystal-growth morphologies, our system may serve as a model problem to understand the influence of long-scale forcing and the effect of the geometry in other physical contexts.

In the following sections we start the formulation by incorporating the flow into the morphological model. The eigenvalue systems are solved to obtain the flow-induced patterns and stability threshold. A WKB theory gives the asymptotic structures of the localized morphologies. A brief summary closes our presentation.

2. Flow-modified interfacial dynamics

During the directional solidification of a binary alloy, the planar solid–liquid interface becomes unstable when the pulling speed is greater than a critical value, at which point cellular patterns form on a length scale $2\pi/\beta_c$ determined by the material properties and operating conditions. This instability is driven by the adverse concentration gradient created by solute rejection at the solid–liquid interface. The linear stability analysis of Mullins & Sekerka (1964) gives the neutral stability curve and the minimum in the graph of morphological parameter M versus wavenumber β. The morphological number M is proportional to the local concentration gradient and, hence, the pulling speed.

Near the minimum (M_c, β_c) we can approximate the dispersion relation by the equation

$$\sigma + (\beta_c^2 - \beta^2)^2 = M - M_c \tag{2.1}$$

when employing appropriate physical length and time scales. Here, σ represents the growth rate. Equation (2.1) is written as a function of β^2, reflecting the rotational symmetry of the planar solution. It also indicates the exchange of stability at the critical point, which was demonstrated by Wollkind & Segel (1970). In terms of the interfacial shape disturbance $h(\boldsymbol{x}, t)$, where $\boldsymbol{x} = (x, y)$, the dispersion relation can be reformulated as

$$\frac{\partial h}{\partial t} + (\beta_c^2 + \nabla^2)^2 h = (M - M_c)h. \tag{2.2}$$

When appropriate nonlinearities are appended (see, for example, Cross & Hohenberg 1993), this governs the modelling of the nonlinear interfacial behaviour in directional solidification.

We consider the morphological instability perturbed by a pre-existing cellular convective field. The flow strength is denoted by a parameter δ and flow spatial scale by $2\pi/\alpha$. In practice, such flows may arise from hydrodynamic or solutal-buoyancy instability; the flows usually have much longer length scales than that of the morphological cells (Coriell *et al.* 1980). Therefore, we shall consider the case of $\alpha \ll \beta_c$ in our analysis. When the flow strength δ and the perturbed morphological number $m = M - M_c$ are small, instability of the moving front is a perturbation from the pure solidification problem, and the interfacial dynamics can be modelled by

$$\frac{\partial h}{\partial t} + (1 + \nabla^2)^2 h + \delta \boldsymbol{u} \cdot \nabla h = (m + \delta \chi w) h, \tag{2.3}$$

in which we have neglected the higher-order terms and set $\beta_c = 1$ without loss of generality, since only α/β_c matters. The transport in the z-direction (normal to the free surface) has been factored out so that the velocity components $\boldsymbol{u}$ and w are projections with respect to the average crystal front. Equation (2.3) is a Mullins–Sekerka problem with a forced convection near the marginal stability limit. The vector field $\boldsymbol{u}(\alpha \boldsymbol{x})$ represents flow components tangential to the crystal plane, convecting disturbances downstream. The normal component $w(\alpha \boldsymbol{x})$ modifies the morphological number through a scaling parameter $\chi > 1$, which measures the boundary-layer thickness of the flow. The parameter χ has been computed for the case of roll-like convective field (Chen & Davis 1999), in which the corresponding slow-variable dynamics had been obtained through the solute conservation law and momentum transport equation using multiple-scale analysis. Equation (2.3) can then be derived by regrouping the slow- and fast-variable dynamics in the linear regime. Here, we shall look at the influence of more complicated flows and employ (2.3) to depict the flow-modified problem in general. The flow strength δ is proportional to the magnitude of velocity in the far field and $0 < \alpha \ll 1$. By setting $\delta = 0$ the formulation has an eigensolution $e^{i\boldsymbol{\beta}\cdot\boldsymbol{x}+\sigma t}$, with a dispersion relation given by (2.1).

We shall consider a class of cellular convective fields whose flow components satisfy the following equations:

$$\nabla^2 w + \alpha^2 w = 0, \tag{2.4}$$

$$\alpha^2 \boldsymbol{u} = \nabla w. \tag{2.5}$$

This type of fluid motion is motivated by the cellular-flow profiles near the onset of hydrodynamic or buoyancy instability (Chandrasekhar 1961). The connection between the two formulae is simply kinematic and required by the conservation of mass. The previously studied roll flow (Chen & Davis 1999) for example, has the profile $w = \alpha \cos(\alpha x)$ and $\boldsymbol{u} = (-\sin \alpha x, 0)$, which is a special case in this category. For three-dimensional flow systems, the flow fields can be expressed as compositions of rolls with wave vectors $\boldsymbol{k}_j$ of different orientations:

$$w(\alpha x, \alpha y) = \frac{\alpha}{N} \sum_{j=1}^{N} \cos(\alpha \boldsymbol{k}_j \cdot \boldsymbol{x}), \quad |\boldsymbol{k}_j| = 1, \tag{2.6}$$

and the corresponding $\boldsymbol{u}$ is derived from (2.5). The flow field is arranged such that $|\boldsymbol{u}| = O(1)$ and the origin is located at one of the convergent flow-stagnation points. The normal-flow component, $w = O(\alpha)$, is further amplified by the factor χ in the

interfacial dynamics. Examples in addition to the roll flow are square and hexagonal patterns which may occur in directional solidification experiments,

$$\text{roll:} \quad N = 1, \quad \boldsymbol{k}_1 = (1,0); \tag{2.7}$$

$$\text{square:} \quad N = 2, \quad \boldsymbol{k}_1 = (1,0), \quad \boldsymbol{k}_2 = (0,1); \tag{2.8}$$

$$\text{hexagon:} \quad N = 3, \quad \boldsymbol{k}_1 = (1,0), \quad \boldsymbol{k}_2 = (-1/2, \sqrt{3}/2), \quad \boldsymbol{k}_3 = (-1/2, -\sqrt{3}/2). \tag{2.9}$$

Equation (2.3) depicts the early-stage development of an infinitesimal disturbance until the effects of the nonlinear terms set in. Its solutions predict the stability boundary and possible morphological patterns for the flow-modified problem. For convenience we shall study the normal mode: $h(x,y,t) \mapsto \mathrm{e}^{\mathrm{i}\omega t} h(x,y)$, and consider the neutrally stable solutions only (ω real). The deduced system,

$$(1+\nabla^2)^2 h + \delta \boldsymbol{u} \cdot \nabla h - \delta \chi w\, h = (m - \mathrm{i}\,\omega) h, \tag{2.10}$$

is a two-dimensional Floquet problem in which the periodic coefficients have slow spatial variations inherited from the cellular-flow profiles. We are interested in the spatially bounded solutions (i.e. eigensolutions), including solutions that are commensurate (harmonic–subharmonic) and incommensurate (aperiodic) with the flow periodicity. Their structures are investigated in different parameter regimes.

3. Resonance condition

When the flow is relatively weak, we express the solution as a regular expansion of δ,

$$h(\boldsymbol{x};\delta) = h_0(\boldsymbol{x}) + \delta h_1(\boldsymbol{x}) + \delta^2 h_2(\boldsymbol{x}) + \cdots, \tag{3.1}$$

and exclude cases in which small divisors may appear. We investigate its uniformity by substituting (3.1) into the linear problem (2.10), and solving for $h_j(x,y)$ at each order of δ. Results for the leading-order system are

$$h_0 = \mathrm{e}^{\mathrm{i}\boldsymbol{\beta}\cdot\boldsymbol{x}} + \text{c.c.}, \quad (1-\beta^2)^2 = m, \tag{3.2}$$

which corresponds to the cellular solution of the classical Mullins–Sekerka instability; c.c. represents complex conjugate. Here, we have absorbed $\mathrm{i}\,\omega$ into m, and assumed that $|m|$ is not as small as δ so that it is retained in the $O(1)$ equation. At this order the solutions are superposition of rolls defined by (3.2).

At $O(\delta)$ we obtain

$$(1+\nabla^2)^2 h_1 - m h_1 = \chi w h_0 - \boldsymbol{u} \cdot \nabla h_0, \tag{3.3}$$

in which the right-hand side shows interaction between the flow and morphological cells that produces perturbation terms like $\mathrm{e}^{\mathrm{i}(\boldsymbol{\beta} \pm \alpha \boldsymbol{k}_j)\cdot\boldsymbol{x}}$. To this order, the flow and cells resonate provided that the oscillatory functions are in the null space of the Mullins–Sekerka operator; that is, if $(1 - |\boldsymbol{\beta} \pm \alpha \boldsymbol{k}_j|^2)^2 = m$. This condition has to be solved together with (3.2) and the resulting formula for $\boldsymbol{\beta}$ is

$$\left.\begin{aligned} \boldsymbol{\beta}^+ &= (1 - \tfrac{1}{4}\alpha^2 \pm \sqrt{m})^{1/2}\, \boldsymbol{k}_j^{\perp} + \tfrac{1}{2}\alpha \boldsymbol{k}_j, \\ \boldsymbol{\beta}^- &= (1 - \tfrac{1}{4}\alpha^2 \pm \sqrt{m})^{1/2}\, \boldsymbol{k}_j^{\perp} - \tfrac{1}{2}\alpha \boldsymbol{k}_j, \end{aligned}\right\} \quad j = 1 \cdots N, \tag{3.4}$$

where $\boldsymbol{k}_j^{\perp}$ is a unit vector orthogonal to $\boldsymbol{k}_j$. We shall view (3.4) as the primary resonance condition for it is deduced from the first-order interaction. In this condition the interfacial patterns are composed of short-scale rolls with the structures defined by (3.2) and directions of the wavevectors defined by (3.4). For the roll convection

(2.7) where the flow field is defined by a single wavevector $\boldsymbol{k}_1$, the induced cellular morphology consists of longitudinal rolls. For the square and hexagonal flows (2.8) and (2.9), compositions of rolls responding to the multiple flow vectors $\boldsymbol{k}_j$ will lead to short-scale square and hexagon cells in the morphologies, respectively. For all of the cases, each set of rolls has grooves aligned and modulated by a subharmonic (period π/α) function in the flow directions $\boldsymbol{k}_j$.

The induced patterns quickly become complicated as more terms are considered in the expansion. Higher-order interactions between the flows and morphological cells further generate perturbation functions $e^{i(\boldsymbol{\beta}+\alpha\boldsymbol{K})\cdot\boldsymbol{x}}$, where $\boldsymbol{K}$ is a linear combination of flow vectors $\boldsymbol{k}_j$,

$$\boldsymbol{K} = \sum_j p_j \boldsymbol{k}_j, \tag{3.5}$$

and p_j are integers. Thus, by comparing the perturbation structure with that of the $O(1)$ equation, the higher-order resonance condition can be readily written by replacing the vector $\boldsymbol{k}_j$ with $\boldsymbol{K}$ in (3.4). The deduced condition then suggests that in the small-δ neighbourhood resonant patterns are given by superpositions of rolls with the wave vectors oriented perpendicularly to $\boldsymbol{K}$, along which appear secondary long-scale structures in response to the imposed flows. In higher-order resonance situations the roll convection (2.7) still produces modulated longitudinal rolls, since $\boldsymbol{K}$ remains one-dimensional. Nevertheless, in the cases of square and hexagonal flows the composed $\boldsymbol{K}$ can point in almost every direction along the crystal plane, which implies less restriction on the directions of $\boldsymbol{\beta}$, and that the flows are too weak to organize the patterns in this regime.

It is desirable to examine the lower bound of the resonance set because it demarcates the marginal stability boundary for the flow-modified morphologies. When the flow is weak this can be achieved by also performing a perturbation analysis but allowing m to approach zero. The solutions are again expressed by (3.1) with an additional ansatz, $m = \delta m_1 + \delta^2 m_2 + \cdots$, substituted into the expansion. An analysis shows that there are multiple branches of solutions bifurcating from the origin $(m, \delta) = \boldsymbol{0}$; two classes are identified. The first has the wavenumber written as (3.4) but with $m = 0$ in the formula. Removing the resonance terms and solving for m_j we arrive at two branches of solutions, referred to branch A:

$$\left.\begin{aligned} \text{A1:}\quad h &\sim e^{i(1-\alpha^2/4)^{1/2}\boldsymbol{k}_j^{\perp}\cdot\boldsymbol{x}} \cos(\alpha \boldsymbol{k}_j \cdot \boldsymbol{x}/2) + \text{c.c.}, \\ m &\sim -\tfrac{1}{2}(\alpha\delta/N)(\chi - \tfrac{1}{2}); \end{aligned}\right\} \tag{3.6}$$

$$\left.\begin{aligned} \text{A2:}\quad h &\sim e^{i(1-\alpha^2/4)^{1/2}\boldsymbol{k}_j^{\perp}\cdot\boldsymbol{x}} \sin(\alpha \boldsymbol{k}_j \cdot \boldsymbol{x}/2) + \text{c.c.}, \\ m &\sim \tfrac{1}{2}(\alpha\delta/N)(\chi - \tfrac{1}{2}). \end{aligned}\right\} \tag{3.7}$$

This class of solutions has subharmonic modulations.

In the second category solutions are harmonic with the flows: $h = e^{i\boldsymbol{k}_j^{\perp}\cdot\boldsymbol{x}} F(\boldsymbol{k}\cdot\boldsymbol{\xi}) + \text{c.c.}$, where $\boldsymbol{\xi} = \alpha\boldsymbol{x}$ are the long-scale coordinates. We find that in the limit $|\delta/\alpha^3| \ll 1$, solutions of this branch can be expressed by asymptotic formula (3.8); call it branch B:

$$\left.\begin{aligned} \text{B:}\quad F &\sim 1 + [\delta/(\alpha^3/N)]\,\chi\cos(\boldsymbol{k}_j \cdot \boldsymbol{\xi}), \\ m/\alpha^4 &\sim -\tfrac{1}{2}[\delta/(\alpha^3/N)]^2\chi(\chi - 1). \end{aligned}\right\} \tag{3.8}$$

The marginal stability curves are then determined by the competition between the two sets of solutions, A and B: whichever defines the minimum of m. Comparing the two categories we see that branch-A solutions give the lower bound of the res-

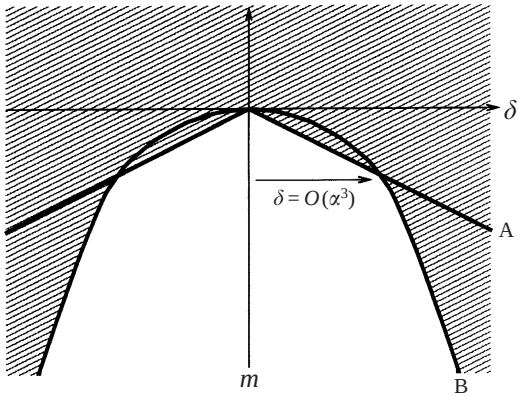

FIGURE 1. Sketch of the branching structure of the resonant solutions. Shaded regions represent unstable states.

onance solutions and, therefore, form the marginal stability boundaries m_c as $\delta \to 0$. Branch B solutions in this weak-flow regime have higher morphological numbers, hence are less dangerous. The asymptotic formulae thus indicate that since $m_c < 0$ the imposed flows promote morphological instability. It is the flow component normal to the free surface that is responsible for the destabilization ($\chi > 1$). The induced patterns are superpositions of (3.6) and (3.7), forming modulated cells in response to orientations of $\boldsymbol{k}_j$. Figure 1 sketches this bifurcation structure near the origin of the (m, δ)-plane.

Further investigation shows that the above result is adequate only in a narrow regime $|\delta/\alpha^3| \ll 1$, where the flows are extremely weak. As the flows get stronger, solutions that continue from branch B become dominant and comprise the marginal stability curves (see figure 1). This switch-over occurs when δ/α^3 is not small so that the regular expansion (3.8) is inappropriate. The behaviour can be understood by using the roll-flow case as an example, in which we let $h = \mathrm{e}^{\mathrm{i}y}F(\xi) + \text{c.c.}$, $\xi = \alpha x$ in (2.10) and the function $F(\xi)$ satisfies

$$-\frac{\alpha^3}{\delta}\frac{\mathrm{d}^4F}{\mathrm{d}\xi^4} + \left(\frac{m}{\alpha\delta} + \chi\cos\xi\right)F + \sin\xi\frac{\mathrm{d}F}{\mathrm{d}\xi} = 0. \tag{3.9}$$

It is clear that when $|\delta/\alpha^3| \gg 1$, the fourth-order term has a small coefficient so that the solutions are non-uniform in this limit. Chen & Davis (1999) have studied this equation and shown that the critical morphological number in this regime is

$$\text{B (continuation)}: \quad m \sim -|\alpha\delta|(\chi - 1), \quad |\delta/\alpha^3| \gg 1. \tag{3.10}$$

The solutions have exponentially localized structures instead of weak modulations of morphological rolls. Thus for $\chi > 1$ the marginal stability curve m_c switches from branch A to branch B (continuation) at $\delta = O(\alpha^3)$.

4. Harmonic balance and WKB approximation

For general δ and m, we seek eigensolutions of (2.10) by the method of harmonic balance. We first employ the flow scale $\boldsymbol{\xi} = (\xi, \eta)$ and rewrite the linear eigenvalue problem (2.10) in a standard form: $\mathrm{L}h = \lambda h$, in which the linear operator L and

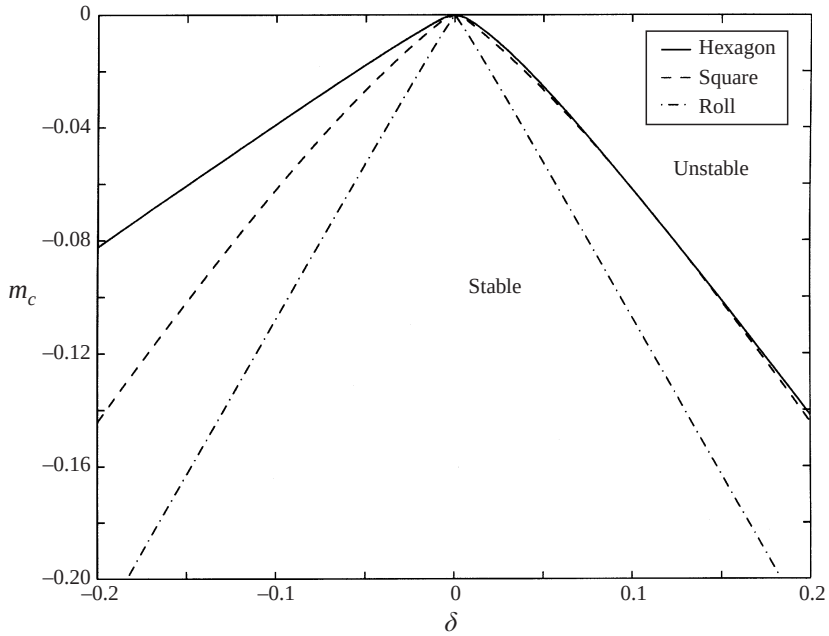

FIGURE 2. Marginal stability boundaries computed by the harmonic-balance method. $\chi = 10$ and $\alpha = 0.125$ for each case.

eigenvalue λ are defined as

$$\mathrm{L} = (1 + \alpha^2 \nabla_\xi^2)^2 + \alpha\delta \boldsymbol{u} \cdot \nabla_\xi - \delta\chi w, \tag{4.1}$$

$$\lambda = m - \mathrm{i}\,\omega, \tag{4.2}$$

and $\nabla_\xi = (\partial_\xi, \partial_\eta)$. In this formulation we have viewed the morphological number m and the frequency ω, respectively, as the real and imaginary parts of the eigenvalue λ. Solutions that are commensurate with the flows are expressed as harmonic expansions in both the ξ- and η-directions, corresponding to the cellular flow patterns (2.7) to (2.9),

$$\text{roll \& square:} \quad h(\xi,\eta) = \sum_p \sum_q A_{pq} \exp[\mathrm{i}\,(\tfrac{1}{2}p\xi, \tfrac{1}{2}q\eta)], \tag{4.3}$$

$$\text{hexagon:} \quad h(\xi,\eta) = \sum_p \sum_q A_{pq} \exp[\mathrm{i}\,(\tfrac{1}{4}p\xi, \tfrac{1}{4}\sqrt{3}q\eta)]. \tag{4.4}$$

Here, p and q are integers, with even values of (p,q) representing the harmonic solutions and odd values the subharmonic (period-doubling) solutions. Similar types of expansions have been widely used to solve parametric-excitation systems of a single degree of freedom, and the convergence has also been studied extensively (e.g. see Karpeshina 1997 and the references therein).

Formally, we substitute expansions (4.3) and (4.4) into the linear eigenvalue problem, collect coefficients of like terms and obtain a set of relations connecting the amplitudes A_{pq}:

$$\sum_i \sum_j L_{pq}^{ij} A_{ij} = \lambda A_{pq}. \tag{4.5}$$

This system is solved numerically by a standard eigenvalue solver (LAPACK 1999) with

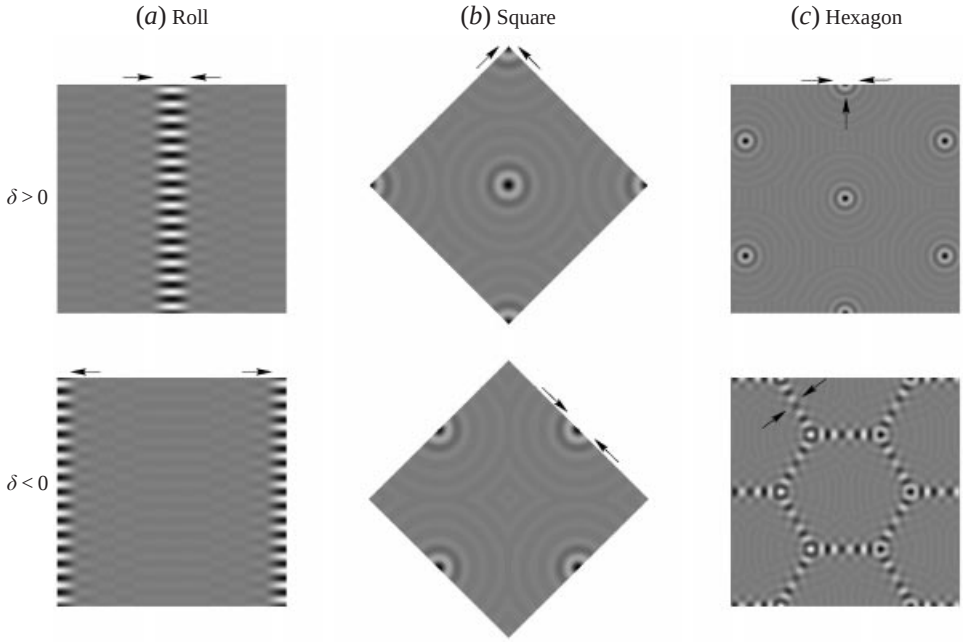

FIGURE 3. Localized patterns produced by the cellular convective fields. The patterns are expected to be seen when $|\delta/\alpha^3| \gg 1$. Here, arrows indicate flow directions near the crystal plane. The gray scale represents the height of the interfacial patterns.

chosen parameters (δ, α, χ) and upper–lower bounds of summing indices. We perform this calculation for the flow patterns listed. Of particular interest is the identification of the minimal $\mathrm{Re}(\lambda) = m_c$, which represents the critical morphological number for the flow-modified systems.

Figure 2 summarizes the marginal stability boundaries obtained from the numerical calculations. It is seen that the imposed flows are destabilizing ($m_c < 0$) in general, which is in agreement with the analysis in the previous section. In the small-(δ, α) parameter regime those marginal stability solutions are stationary in time ($\omega = 0$), in contrast with the travelling wave solutions ($\omega \neq 0$) in the two-dimensional morphology (Chen & Davis 1999). The roll-like convection has a stronger destabilizing effect than the square and hexagonal flows for a given pair of flow parameters. By inspecting the numerical results we observe that all of the cellular flows perturb the stability boundaries weakly: given a small but finite δ the computed m_c approaches zero as $\alpha \to 0$. Those minima follow branch A near the origin in the (m, δ)-plane, but quickly deviate from the curves when the value of δ/α^3 increases, showing the branching structure sketched in figure 1. Solutions of the roll flow then agree with the branch B (continuation); the square and hexagonal flow cases also exhibit similar behaviour.

Our computations thus show that, though the stability boundaries are only weakly perturbed, the morphological structures can be strongly modified. Figure 3 plots the interfacial patterns of those marginally stable solutions in the strong-flow limit, $|\delta/\alpha^3| \gg 1$. In this regime the flows produce spatially localized morphologies, in which interfacial disturbances are confined to the convergent flow-stagnation regions. When the local flow field converges to a point the induced pattern shows a focus-like local structure, while if the flow converges to a line the local pattern becomes ridge-like. For roll and square convective fields the localized patterns form arrays and clusters

on the crystal plane, respectively (figures 3*a* and 3*b*). Switching parity of the flows ($\delta \to -\delta$) is equivalent to a translation of coordinates, producing the same type of morphology and the same stability boundaries. In contrast, a hexagonal convection does not possess this symmetry. An inward hexagonal flow ($\delta > 0$) produces localized foci at the centres of hexagonal flow cells, whereas an outward flow ($\delta < 0$) produces localized ridges at the rims of each hexagon (figure 3*c*). This asymmetry is also indicated in the plot of the marginal stability curve (figure 2), which shows that the inward hexagonal flow has a stronger destabilizing effect than the outward case. In summary, in this strong-flow regime structures of the localized patterns are determined by the local flow fields. Their arrangements on the front follow the spatial variation of the cellular flow profiles.

Away from the marginal stability limits the eigensolutions also exhibit localized structures. They are higher-order modes corresponding to further phase distortion or symmetry breaking of the local patterns. For example, in the case of inward hexagonal flows, broken-symmetry resulting in 'flower'-like patterns is observed at the convergent stagnation points; a few of these are shown in figure 4. Those higher-order solutions have eigenvalues larger but not far from the marginal stability limit m_c, due to the long flow periods (small α). Thus, in practice, when the morphological number m is raised into the unstable regime many such modes will be excited together with the marginal stability solution. In this case nonlinear competition between those localized states will determine the actual pattern seen in experiment.

We investigate the asymptotic structures of those localized solutions by looking at the local form of (2.10) near the convergent flow-stagnation regions. For the focus-type pattern we expand the flow functions near the origin, so that the flow contributions are written as

$$\left.\begin{aligned} \delta \boldsymbol{u} \cdot \nabla h &\sim -\frac{1}{2}\,\alpha\delta \left(\xi \frac{\partial}{\partial \xi} + \eta \frac{\partial}{\partial \eta}\right) h, \\ \delta \chi w h &\sim \alpha\delta\chi\,[1 + O(\xi^2 + \eta^2)]h, \end{aligned}\right\} \tag{4.6}$$

where $|\xi|$ and $|\eta|$ are small. This formula suggests that we seek a shape function of the form: $h \mapsto \mathrm{e}^{\mathrm{i}n\theta} h(r) + \text{c.c.}$, satisfying (2.10) with the flow contributions replaced by the local formula (4.6). Here, $r^2 = \xi^2 + \eta^2$, θ is the phase angle, and n an integer. In cylindrical coordinates the interfacial morphology near the convergent stagnation point is written

$$\left[1 + \frac{\alpha^2}{r}\frac{\mathrm{d}}{\mathrm{d}r}\left(r\frac{\mathrm{d}}{\mathrm{d}r}\right) - \frac{n^2\alpha^2}{r^2}\right]^2 h - \frac{1}{2}\,\alpha\delta r \frac{\mathrm{d}h}{\mathrm{d}r} = (\lambda + \alpha\delta\chi)\,h. \tag{4.7}$$

Equation (4.7) governs the local morphologies for both square and inward hexagon flows. We note the close proximity of the two marginal stability curves in this strong-flow regime (figure 2), which implies that the induced morphologies of the two flows can be approximated by the same equation locally.

It is readily seen that, in the no-flow situation, the formulation has an eigensolution written in terms of a Bessel function

$$h(r) = \mathrm{J}_n(r/\alpha) \sim \left(\frac{2\alpha}{\pi r}\right)^{1/2} \cos(r/\alpha - \tfrac{1}{2}n\pi - \tfrac{1}{4}\pi) \tag{4.8}$$

at the onset of pure Mullins–Sekerka instability ($\lambda = 0$), in which the fast oscillatory function represents short-scale morphological cells. In the presence of the flows we express $h(r)$ as a function consisting of the short-scale cells and a WKB-type envelope

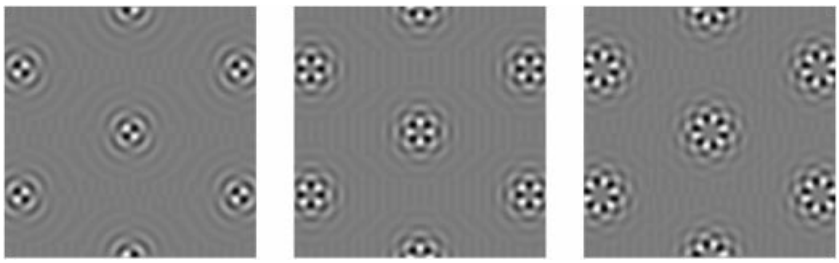

FIGURE 4. Higher-order localized states produced by the inward hexagonal flow fields.

function

$$h(r) = r^{-1/2}\,\mathrm{e}^{\mathrm{i}r/\alpha}\,\mathrm{e}^{[S(r)/\epsilon]} + \text{c.c.}, \tag{4.9}$$

in which $\epsilon \ll 1$ is a scaling parameter. We find a locally exponential envelope when choosing $\epsilon = (\alpha^2/\delta)^{1/2}$, and the function $S(r)$ satisfies (to the leading order)

$$\left(\frac{\mathrm{d}S}{\mathrm{d}r}\right)^2 + \frac{\mathrm{i}}{8}r = 0, \tag{4.10}$$

which results in two branches of solutions: $S = \pm\frac{1}{6}(1-\mathrm{i})r^{3/2}$. Suppressing the growing mode we arrive at an approximation for the structure of a focus:

$$h \propto r^{-1/2}\mathrm{e}^{\mathrm{i}r/\alpha}\exp[-\tfrac{1}{6}(1-\mathrm{i})(\delta/\alpha^2)^{1/2}r^{3/2}] + \text{c.c.} \tag{4.11}$$

The solution is appropriate in the intermediate regime, $(\alpha^2/\delta)^{1/3} \ll r \ll 1$, where both (4.6) and (4.10) are valid.

Similarly, we write the ridge-like localization as short-scale morphological cells plus an envelope function: $h = \mathrm{e}^{\mathrm{i}\eta/\alpha}\,\mathrm{e}^{\mathrm{i}n\alpha\eta}F(\xi) + \text{c.c.}$, where $n = O(1)$. For the roll convection this decomposition is straightforward and $F(\xi)$ satisfies

$$-\frac{\alpha^3}{\delta}\left(\frac{\mathrm{d}^2}{\mathrm{d}\xi^2} + 2n + n^2\alpha^2\right)^2 F + \left(\frac{\lambda}{\alpha\delta} + \chi\right)F + \xi\frac{\mathrm{d}F}{\mathrm{d}\xi} = 0. \tag{4.12}$$

The case of $n = 0$ is the local form of (3.9). By employing a WKB-type approximation and selecting the decaying branch, we obtain

$$F \propto \exp[-(\delta/\alpha^3)^{1/3}(\tfrac{1}{8}\sqrt{3} - \tfrac{3}{8}\sqrt{3}\,\mathrm{i}\,)\,\xi^{4/3}], \quad (\delta/\alpha)^3 \gg 1, \tag{4.13}$$

which is valid in the regime $(\alpha^3/\delta)^{1/4} \ll \xi \ll 1$.

For the case of outward hexagonal flow (figure 3*c*, $\delta < 0$) the analysis is complicated by the non-simple flow along the rims. Nevertheless, the ridge-like morphology suggests that equation (4.12), with an adjusted flow magnitude, may serve as an approximation to the local pattern and hence determines the scaling of the envelope. The (ξ, η) coordinates here will have to be rearranged such that they are measured from the centre of a ridge, respectively parallel and orthogonal to the converging flow direction. Also, near the corners where three neighbouring ridges meet, the local flow converges to a point and produces focus-type patterns; equation (4.7) may be appropriate to describe the local structures. Thus, the morphology along the rims can then be constructed by patching the ridge and focus patterns. Detailed matching has not been carried out.

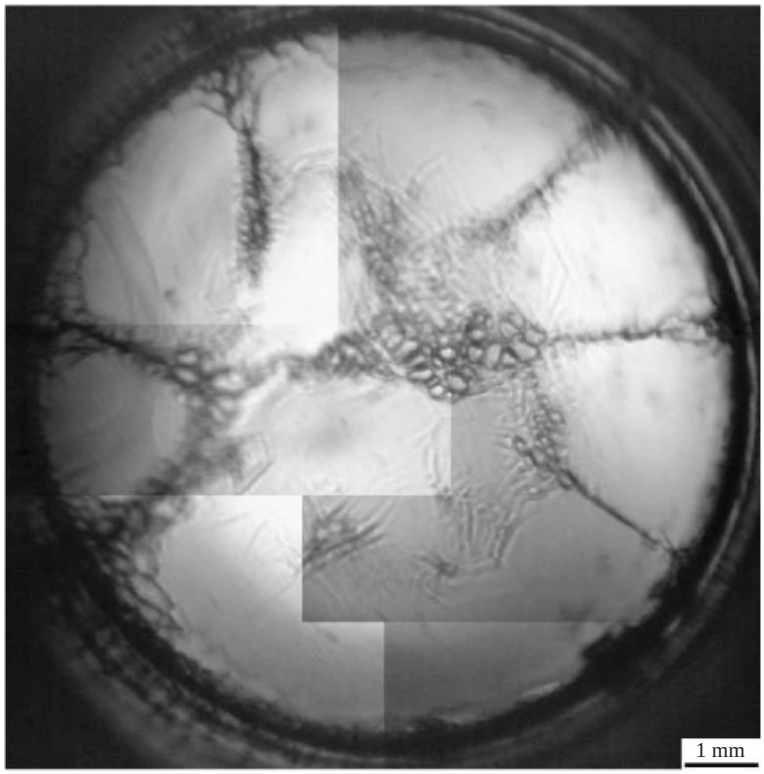

FIGURE 5. Direct observation from above of the localized morphology induced by thermo-solutal-driven convection. Patterned area indicates morphological instability and corresponds to convergent flow-stagnation regions near the crystal plane. A transient state of solidification 67 minutes after the growth of succinonitrile–0.2 wt% acetone alloy with $V = 1.5\,\mathrm{mm\,s^{-1}}$ and thermal gradient $G = 30\,\mathrm{C^{\circ}\,cm^{-1}}$. Photo from Jamgotchian *et al.* (2000).

5. Summary

Our investigation, extending previous analysis on the two-dimensional convection case (Chen & Davis 1999), focuses on the induced morphologies in three-dimensional flow systems. The interfacial dynamics is based on the classical Mullins–Sekerka problem in directional solidification, but includes the effect of fluid motion in the model equation. The imposed flows have spatial wavenumber α and strength parameter δ, which control the perturbation from the pure morphological instability. The dynamical system has a multi-dimensional, parametric-excitation structure. Linear theory reveals the flow-induced morphologies and marginal stability boundaries. WKB analysis delivers the scalings of the localized states. The spatial localization is due to solute redistribution by the fluid motions. The imposed flows convect inhomogeneities to convergent flow-stagnation regions and promote instability locally. Length scales of the local patterns are determined by the balance between interfacial flow and surface-tension forces. The flows strongly control the patterns when $|\delta/\alpha^3| \gg 1$.

We analyse the effect of spatially periodic flows on growing crystal fronts. Since the local flow profiles in the vicinity of stagnation regions can be classified and analysed, the insight gained from the current analysis on the cellular flows presents a way to understand the flow-induced morphologies in complex flows. We note that

an early experiment performed by Hämäläinen (1967) has shown that morphological instability occurs first at the corners of convection cells. Experiments by Jamgotchian *et al.* (2000) have also demonstrated localized interfacial morphologies in the flow convergent regions even when the flows are not spatially periodic; see figure 5. Various physical systems with similar mathematical structures are mentioned in §1, which, when extended to multi-dimensional cases, may show results that qualitatively agree with ours. In Class's study on cellular flame combustion (Class *et al.* 1998; Class 2000, personal communication), for example, he has observed localized flame patterns similar to figures 3 and 4, though the physics that drives the instability is distinctively different from that in the present case.

This work was supported by NASA, Microgravity Sciences and Application Programs. We thank Dr H. Jamgotchian for providing figure 5.

REFERENCES

Brattkus, K. & Davis, S. H. 1988 *J. Cryst. Growth* **89**, 423.

Bühler, L. & Davis, S. H. 1998 *J. Cryst. Growth* **186**, 629.

Chandrasekhar, S. 1961 *Hydrodynamics and Hydromagnetic Stability*. Oxford University Press.

Chen, Y.-J. & Davis, S. H. 1999 *J. Fluid Mech.* **395**, 253.

Class, A. G., Bühler, L. & Davis, S. H. 1998 *Phys. Rev. Lett.* **80**, 4414.

Connor, J. N. L., Uzer, T., Marcus, R. A. & Smith, A. D. 1984 *J. Chem. Phys.* **80**, 5095.

Coriell, S. R., Cordes, M. R., Boettinger, W. S. & Sekerka, R. F. 1980 *J. Cryst. Growth* **49**, 13.

Coriell, S. R., McFadden, G. B. & Boisvert, R. F. 1984 *J. Cryst. Growth* **69**, 15.

Cross, M. C. & Hohenberg, P. C. 1993 *Rev. Mod. Phys.* **65**, 851.

Davis, S. H. 1993 In *Handbook of Crystal Growth* (ed. D. T. J. Hurle), vol. 1 ch. 13, p. 861. Elsevier.

Eckhaus, W. & Kuske, R. 1997 *SIAM J. Appl. Maths* **57**, 112.

Forth, S. A. & Wheeler, A. A. 1989 *J. Fluid Mech.* **202**, 339.

Hämäläinen, M. 1967 *J. Cryst. Growth* **1**, 125.

Höbbs, A. K. & Metzener, P. 1991 *J. Cryst. Growth* **112**, 539.

Jamgotchian, H., Bergeon, N., Benielli, D., Voge, Ph., & Billia, B. 2000 Convection-induced microstructures and microstructure-induced convection in directional solidification. *EUROMECH Colloquium 408: Interactive Dynamics of Convection and Solidification, March 2000, Chamonix, France.*

Karpeshina, Y. E. 1997 *Perturbation Theory for the Schrödinger Operator with a Periodic Potential.* Springer

Lapack 1999 *Lapack User's Guide*, 3rd Edn. SIAM

Mullins, W. W. & Sekerka, R. F. 1964 *J. Appl. Phys.* **35**, 444.

Pal, D. & Kelly, R. E. 1979 *ASME Paper* 79-HT-109.

Schulze, T. P. & Davis, S. H. 1994 *J. Cryst. Growth* **143**, 317.

Schielen, R. & Doelman, A. 1998 *SIAM J. Appl. Maths* **58**, 1901.

Walton, I. C. 1982 *Q. J. Mech. Appl. Maths* **35**, 33.

Wollkind, D. J. & Segel, L. A. 1970 *Phil. Trans. R. Soc. Lond.* A **268**, 351.